

Analysis of Simultaneous Transformation and Plastic Deformation in Shape Memory Alloys

D. J. Hartl and D. C. Lagoudas

Texas A&M University, College Station, TX, U.S.A.

ABSTRACT

The new developments summarized in this work represent both experimental and theoretical investigation of the effects of plastic strain generation in Shape Memory Alloys (SMAs). Based on the results of SMA experimental characterization described in the literature and additional testing described in this work, a new 3-D constitutive model is proposed. This phenomenological model captures both the conventional shape memory effects of pseudoelasticity and thermal strain recovery, and additionally considers the initiation and evolution of plastic strains. The theoretical model is numerically implemented in a finite element framework using return mapping algorithms to solve the constitutive problem at each material point. This combination of theory and implementation is unique in its ability to capture the simultaneous evolution of recoverable transformation strains and irrecoverable plastic strains. The consideration of isotropic and kinematic plastic hardening provide the theoretical framework for capturing the interactions between accumulated plastic strain and martensitic transformation. The model has been used to perform 3-D analysis of SMA structural components in bending. Experimentally validated results considering simultaneous transformation and plasticity are provided.

Keywords: shape memory alloys, SMA, Nitinol, plastic yield, constitutive modeling, FEA, active materials, smart structures

1. INTRODUCTION

The constitutive modeling of Shape Memory Alloys (SMAs)^{1,2} has traditionally focused on capturing the elastic and transformation behaviors of the material. Many models exist which can account for the generation and recovery of inelastic deformation resulting from the martensitic transformation and these are suitable for modeling the response of conventional SMAs as used in multi-use applications. However, as SMAs are more commonly being formed into complex shapes and used at higher temperatures (so-called high temperature SMAs),³ the need to also accurately account for irrecoverable inelastic strains has become increasingly important.

Past work on irrecoverable plastic strain generation in SMAs has focused on two distinct phenomena. The first is known as transformation-induced plasticity (TRIP) while the second is associated with slip mechanisms which initiate at sufficiently high stresses (i.e., yield stresses). TRIP accounts for irrecoverable strain generated due to the cyclic thermomechanical transformation of shape memory alloys during which dislocations, grain boundary mismatches, and other effects can accumulate.^{4,5} A non-negligible permanent macroscopic deformation (relative to the original reference configuration) is observed. Modeling of this plastic behavior does not include the conventional notion of a yield surface, but rather proposes evolution equations for the plastic variables which are strictly dependent on the number of transformation cycles completed.

The second type of SMA constitutive model accounting for irrecoverable strains combines known phenomenological SMA models with conventional metal plasticity formulated using yielding surfaces in stress space. Such models have been formulated in 1-D,^{6,7} 2-D,⁸ and 3-D.⁹ However, the current models, in the forms presented in the literature, are intended to address permanent plastic yield which occurs *outside* of active transformation regions (e.g., after forward stress-induced transformation has ended). Modeling of simultaneous transformation and yield has not been considered in the literature.

Our current research effort involves experimental investigation and theoretical modeling of rate-independent inelasticity in SMAs and accounts for simultaneous transformation and plastic strain generation. Motivated by

Further author information: (Send correspondence to D.C.L.)
E-mail: lagoudas@aero.tamu.edu, Telephone: 1 979 845 9409

experiments briefly summarized herein, an SMA model which additionally captures the formation and evolution of plastic strain in three dimensions has been developed. Material response can be predicted when the plastic deformation is occurring in a pure phase, in mixed phases, or in a material simultaneously undergoing transformation. The model is derived using continuum thermodynamics where appropriate evolution criteria have been chosen and the constraints on dissipation have been considered. Multiple “yield” surfaces are used to capture the transformation and plastic yield behaviors simultaneously.

2. SMA/PLASTIC YIELD CONSTITUTIVE MODEL

While constitutive models and implementations exist which can account for non-simultaneous transformation and yielding, experimental evidence motivates the development of models which address simultaneous processes. Many models accounted for conventional SMA behavior have been developed over the years.² An example of a phenomenological model which is both easily implemented yet of sufficient utility is the unified model proposed by Lagoudas et al.¹⁰ The model accounts for transformation from detwinned martensite to austenite and back again. The full 3-D form of the model has been numerically implemented in the ABAQUS/Standard analysis suite.¹¹ Combination of the unified model with this powerful nonlinear FEA software allows for analysis of complex structures that include active SMA elements.

In the current work, the focus is shifted beyond the conventional SMA model which addresses only martensitic phase transformation. Here, the initiations and evolutions of two distinct dissipative processes are considered. These processes, martensitic transformation and plastic slip, are the results of two very different underlying physical mechanisms and they cause differing thermomechanical material responses. The processes are also coupled in their effects, especially in the manner by which residual plastic deformation alters the transformation characteristics (the critical transformation temperatures and recoverable strain) in subsequent transformation cycles. This work accounts for these changes by utilizing kinematic plastic hardening and introducing an associated *back stress* generated in the same direction as the local plastic strain. This back stress translates both the plastic yield surface and the forward and reverse transformation surfaces and additionally alters the generation of transformation strains. Therefore, the effects of transformation in a post-yielded material can differ sharply from those in the pre-yielded material.

The full thermomechanical model for these behaviors is summarized below. The relations describing the transformation behavior, derived in past works^{10,12} are presented in parallel with the new plastic model relations. Note that this is not meant to be a detailed derivation, but rather a summary as the details of the previously derived thermodynamic SMA model are well explained in the literature.

2.1. Development of Constitutive Relations for Martensitic Transformation and Plastic Yield

The derivation of the new SMA transformation/plasticity model with kinematic hardening begins with the choice of a free energy and complimentary independent state variables (both externally applied and internally evolving). In the manner of Lagoudas and coworkers,² we choose the Gibbs energy. The thermoelastic state variables are then *stress* $\boldsymbol{\sigma}$ and *temperature* T . In following with past models, the internal state variables which track the progression of martensitic transformation are the tensor-valued *transformation strain* $\boldsymbol{\varepsilon}^t$ and the scalar-valued *martensitic volume fraction* ξ . To account for the generation and evolution of plastic deformation, the *plastic strain* $\boldsymbol{\varepsilon}^p$ is introduced, where the isotropic plastic hardening is measured as a function of the *drag stress* η . The kinematic hardening is accounted for by considering the *back stress* $\boldsymbol{\beta}$ which is assumed to track the center of both the transformation and plastic yield surfaces in the six-dimensional stress space. Given these state variables, the Gibbs energy for the overall SMA material (austenite/martensite composite) is then written:

$$\begin{aligned}
 G(\boldsymbol{\sigma}, T, \boldsymbol{\varepsilon}^t, \xi, \boldsymbol{\varepsilon}^p, \eta, \boldsymbol{\beta}) := & - \frac{1}{2\rho} \boldsymbol{\sigma} : \mathcal{S} : \boldsymbol{\sigma} - \frac{1}{\rho} \boldsymbol{\sigma} : \boldsymbol{\alpha} (T - T_0) + c \left[(T - T_0) - T \ln \left(\frac{T}{T_0} \right) \right] - s_0 T + u_0 \\
 & - \frac{1}{2\rho} \frac{1}{K^\beta} \boldsymbol{\beta} : \boldsymbol{\beta} - \frac{1}{\rho} \boldsymbol{\sigma} : [\boldsymbol{\varepsilon}^p + \boldsymbol{\varepsilon}^t] + \frac{1}{\rho} \boldsymbol{\beta} : [\boldsymbol{\varepsilon}^p - \boldsymbol{\varepsilon}^t] + f^t(\xi) + f^p(\xi, \eta). \quad (2.1)
 \end{aligned}$$

The material constants \mathcal{S} , $\boldsymbol{\alpha}$, ρ , c , s_0 and u_0 denote the effective compliance tensor, effective thermal expansion coefficient tensor, density, effective specific heat, effective specific entropy at the reference state, and effective

specific internal energy at the reference state, respectively. Assuming linear kinematic hardening, the back stress β can be shown to be explicitly related to the plastic stress ε^p through the kinematic hardening modulus, here taken to be phase-dependent and given as $K^\beta(\xi)$. The back stress is therefore not an independent variable but rather an explicit function of two other variables. Thus the Gibbs energy can be written $G = G(\sigma, T, \varepsilon^t, \xi, \varepsilon^p, \eta)$. All the material constants included in G are defined in terms of the martensitic volume fraction, ξ , by the rule of mixtures (e.g., $\mathcal{S} := \mathcal{S}^A + \xi(\mathcal{S}^M - \mathcal{S}^A)$, etc).

Application of the first and second laws of thermodynamics via the Coleman-Noll procedure¹³ (not described in detail here) then gives the following relations for the total strain and entropy:

$$\varepsilon = -\rho \partial_{\sigma} G = \mathcal{S} : \sigma + \alpha(T - T_0) + \varepsilon^t + \varepsilon^p, \quad s = -\partial_T G = \frac{1}{\rho} \sigma : \alpha + c \ln \left(\frac{T}{T_0} \right) + s_0. \quad (2.2)$$

The remaining dissipative terms resulting from application of the second law can then be written as

$$\left(-\rho \partial_{\varepsilon^t} G : \dot{\varepsilon}^t - \rho \partial_{\xi} G \dot{\xi} \right) + \left(-\rho \partial_{\varepsilon^p} G : \dot{\varepsilon}^p - \rho \partial_{\eta} G \dot{\eta} \right) \geq 0. \quad (2.3)$$

Here we postulate evolution equations for the two tensorial internal state variables ε^t and ε^p in terms of the rates of the two scalar quantities ξ and η . The proposed forms are consistent with the evolution equations (or “flow laws”) commonly used in classical rate-independent plasticity with Mises-type (J_2 -type) yield surfaces^{14, 15} and are given as follows:

$$\dot{\varepsilon}^t = \dot{\xi} H \frac{3}{2} \frac{\sigma_t^{eff'}}{\bar{\sigma}_t^{eff}} = \dot{\xi} \Lambda^t; \quad \dot{\varepsilon}^p = \dot{\eta} \frac{1}{K^\eta} \frac{3}{2} \frac{\sigma_p^{eff'}}{\bar{\sigma}_p^{eff}} = \dot{\eta} \Lambda^p \quad (2.4)$$

where we define back stress as a function of plastic strain as

$$\beta = K^\beta(\xi) \varepsilon^p. \quad (2.5)$$

The two inelastic strains are assumed to evolve in the direction of the deviatoric part of the two *effective stresses* and the scalar term $\bar{\sigma}^{eff}$ denotes the Mises equivalent of the effective stress given. Specifically, the following definitions are used:

$$\sigma_t^{eff} = (\sigma + \beta); \quad \sigma_p^{eff} = (\sigma - \beta); \quad \sigma_p^{eff'} = dev(\sigma_p^{eff}); \quad \bar{\sigma}_p^{eff} = \sqrt{3/2 \sigma_p^{eff'} : \sigma_p^{eff'}}$$

where the difference between σ_t^{eff} and $\sigma_t^{eff'}$ is important to accurately match experimental results. The material constant H denotes the maximum transformation strain generated during complete transformation from austenite to martensite. The isotropic plastic hardening moduli is given as K^η .

Substituting the proposed evolution equations into the dissipative inequality (2.3) where the partial derivatives of the Gibbs energy have been calculated, we arrive at

$$[(\sigma + \beta) : \Lambda^t - \rho \partial_{\xi} G] \dot{\xi} + [(\sigma - \beta) : \Lambda^p - \rho \partial_{\eta} G] \dot{\eta} \geq 0. \quad (2.6)$$

The dissipative processes of martensitic transformation ($\dot{\xi} \neq 0$) and plastic yielding ($\dot{\eta} > 0$) can occur separately or, given some loading paths, simultaneously. Satisfying each of the two terms in (2.6) separately implies that the sum total will also be satisfied. These two conditions are written as products of thermodynamic forces and conjugate fluxes, taking the form

$$[(\sigma + \beta) : \Lambda^t - \rho \partial_{\xi} G] \dot{\xi} = \pi^t \dot{\xi} \geq 0; \quad [(\sigma - \beta) : \Lambda^p - \rho \partial_{\eta} G] \dot{\eta} = \pi^p \dot{\eta} \geq 0. \quad (2.7)$$

The two processes can be assumed to begin only when the thermodynamic forces (π^t, π^p) reach critical levels (Y^t, Y^p). Furthermore, the consistency condition of classical rate-independent plasticity requires that

the thermodynamic force (a yield function) remain equal to the complimentary critical force level while the dissipative process is in progress. These conditions allow the definition of transformation/yield surfaces given as

$$\Phi^t \dot{\xi} = (\pi^t \mp Y^t) \dot{\xi} = \{[(\boldsymbol{\sigma} + \boldsymbol{\beta}) : \boldsymbol{\Lambda}^t - \rho \partial_{\xi} G] \mp Y^t\} \dot{\xi} = 0, \quad (2.8)$$

$$\Phi^p \dot{\eta} = (\pi^p - Y^p(\xi)) \dot{\eta} = \{[(\boldsymbol{\sigma} - \boldsymbol{\beta}) : \boldsymbol{\Lambda}^p - \rho \partial_{\eta} G] - Y^p(\xi)\} \dot{\eta} = 0, \quad (2.9)$$

where the “ \mp ” accounts for forward/reverse transformation, respectively.

To complete the formulation of the SMA transformation/plasticity model, the form of the *hardening functions* must be considered. These are present in the Gibbs free energy (2.1) as $f^t(\xi)$ and $f^p(\xi, \eta)$ for transformation and plastic yield, respectively. The transformation hardening function is given as²

$$f^t(\xi) = \begin{cases} \frac{1}{2} a_1 \left(\xi + \frac{\xi^{n_1+1}}{(n_1+1)} + \frac{(1-\xi)^{n_2+1}}{(n_2+1)} \right) & ; \quad \dot{\xi} > 0 \\ \frac{1}{2} a_2 \left(\xi + \frac{\xi^{n_3+1}}{(n_3+1)} + \frac{(1-\xi)^{n_4+1}}{(n_4+1)} \right) & ; \quad \dot{\xi} < 0. \end{cases} \quad (2.10)$$

This form provides an arbitrarily smooth transformation response based on the parameters n_i . The hardening function for plastic yield is assumed to have a decaying exponential form as suggested in the literature but where the original form has been modified to account for the evolution of material yield properties with changing phase.¹⁴

$$f^p(\xi, \eta) = \frac{1}{\rho K^\eta} \left[(Y_m(\xi) - Y_0(\xi)) \left(1 + \frac{K^\eta}{C_H} e^{-\frac{C_H}{K^\eta} \eta} - \frac{K^\eta}{C_H} \right) \right] - \frac{1}{\rho K^{\eta^2}} K^\beta(\xi) \eta^2 \quad (2.11)$$

The proposed evolution in material plastic properties ($Y_m(\xi)$, $Y_0(\xi)$, and $\beta(\xi)$) introduce much of the transformation/yield coupling predicted by this model. The first bracketed term in (2.11) provides isotropic hardening of an exponential type. The evolution of the monotonic loading response from an initial yield stress of Y_0 toward a plastic yield plateau at stress level Y_m is consistent with experimental observations. The second term linear in effective stress is proposed in the literature¹⁴ to preserve this exponential form.

The decrease in recoverable martensite with increasing plastic yield must also be addressed. Experimental results which motivated this work (briefly summarized below) seemed to indicate that this effect was much more pronounced when plastic yielding occurred in the austenite phase. In this work, an adjustment is made to the lower bound of ξ (initially 0) such that yielding in austenite and the resulting increase in $\bar{\epsilon}^p$ up to and beyond some critical level drives the lower ξ bound from $0 \rightarrow 1$, at which time transformation can no longer occur. A linear relationship between the lower bound and $\bar{\epsilon}^p$ is assumed.⁸

2.2. Features and Implementation of the Transformation/Plasticity Model

The contribution of this new model is the ability to account for transformation and plasticity simultaneously and to further capture the effects that each of these processes has on the other. The location and evolution (size change and motion) of the transformation and yield surfaces is key to this coupling. To demonstrate this effect, the configuration of the transformation and yield surfaces for plane-stress loading are shown in Figure 1. Here the stress axes are denoted “S1” and “S2” with temperature on the vertical axis. The start and finish bounds of the forward transformation surface are shown in blue and red, respectively, while the plastic surface is shown in gray. The conventional SMA phase diagram is a 1-D reduction of the plane-stress case and is shown on the left. Recall that, in agreement with the phase diagram, the 3-D surfaces for the beginning and ending of forward transformation are tapered in applied stress-temperature space while the plastic yield surface is assumed to be invariant with temperature. Shown are two thermomechanical states for two different loading paths: mechanical loading at $A_s - 20^\circ\text{C}$ (80°C) and mechanical loading at $A_s + 45^\circ\text{C}$ (145°C), where A_s denotes the temperature at which transformation from martensite to austenite initiates at zero stress. Note that these two loading paths will be revisited in the experimental results section below.

Loading at $A_s - 20^\circ\text{C}$ (Figure 1a) results first in stress-induced phase transformation (State A) which, when completed, leads to higher stresses sufficient to cause plastic slip (State B). The back stress resulting from the generation of plastic strain (see (2.5)) causes contrary translation of these surfaces in the stress plane. During unloading, no further plastic strain is generated and the surfaces remain at their new positions. This results in altered transformation behavior in cycles following plastic yield.

A temperature of $A_s + 45^\circ\text{C}$ (Figure 1b) maintains the stability of austenite at higher stress levels, allowing for a condition in which yielding occurs prior to transformation (State A). Further loading leads to simultaneous transformation and plastic slip as the material state lies at the intersection of these surfaces (State B). An experimentally observed effect of transformation/yield surface motion during such simultaneous dissipation is an increased hardening response during loading, as is observed in the experimental results below.

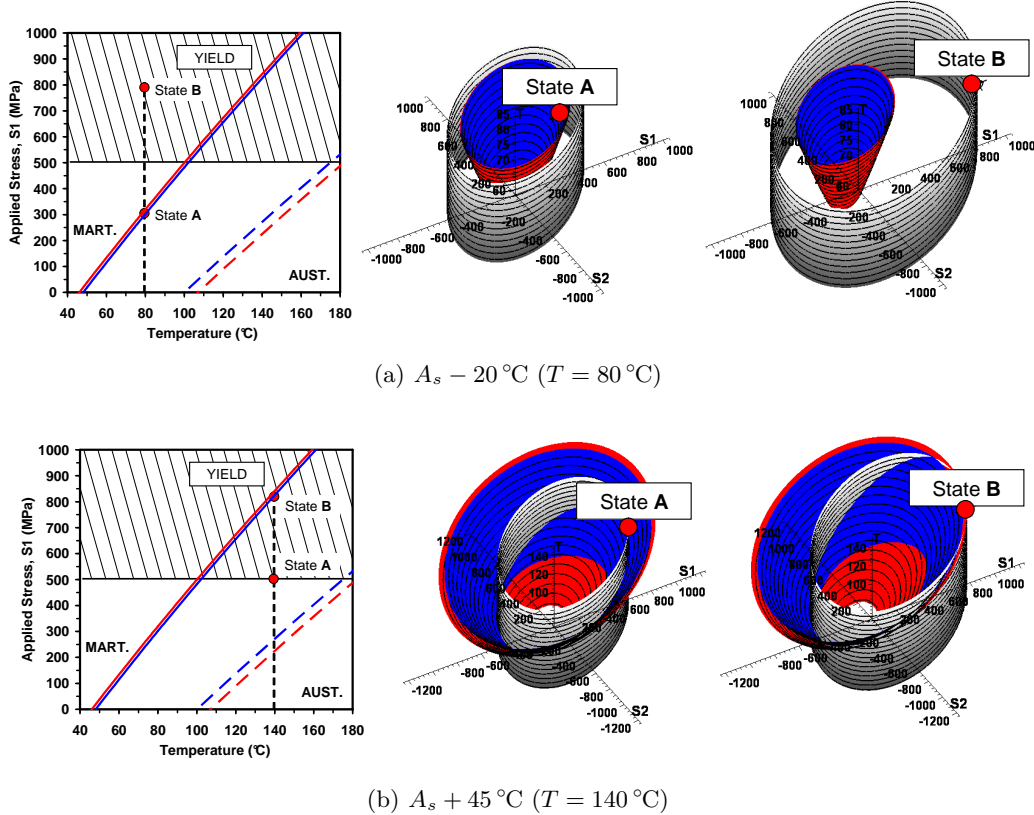


Figure 1. Evolving configuration of transformation and yielding surfaces during pseudoelastic loading at two test temperatures.

Utilization of this model in analyzing the effects of plasticity in engineering applications of SMAs requires the implementation of the combined transformation/plasticity SMA model into an FEA-based numerical framework. For this study, the ABAQUS software suite was chosen as the global solver for the overall structural FEA boundary value problem.¹¹ However, for each integration point of each element during each time step of the incremental solution process, the constitutive model derived above must be used to calculate the stress and internal variable increments for a given strain and temperature increment. In addition, the computed current tangent moduli are also required in support of the global convergence algorithms (i.e. Newton, Quasi-Newton, etc.).

In agreement with the past implementation of the SMA “unified model” (transformation only),¹² a form of *return mapping algorithm* is here modified and used to enforce the consistency condition on Φ^t and Φ^p . To

maintain $\Phi^t = \dot{\Phi}^t = 0$ and $\Phi^p = \dot{\Phi}^p = 0$ during transformation and plastic yield, respectively, the chosen convex cutting plane form of the algorithm iteratively computes the correct stress increment for the given increments $\Delta\varepsilon$ and ΔT . The iterative algorithm takes into account the unique considerations found in the developments of multisurface plasticity.^{14,16} One particular modification to the conventional RMA is that, for a given load increment, violation of a yield (or transformation) surface does not indicate that the complimentary internal variables (plastic strains or transformation strains) are necessarily evolving. One must also check the sign of the resulting increment in the scalar internal variables.

3. MODEL CALIBRATION, ANALYSIS, AND COMPARISON WITH EXPERIMENTAL RESULTS

The model derived above was originally motivated by a qualitative understanding of experimental results for plasticity in SMAs found throughout the literature.^{17,18} Further characterization of SMA material response considering plastic yielding behavior was performed at Texas A&M University to more clearly motivated the new model proposed and to calibrate it in its final form. The elastic behavior, the conventional shape memory behavior, the yielding of pure phases, and the effects of transformation on plasticity and vice versa were assessed.

3.1. Experimental Investigation of Plastic Yield

The material chosen for experimental characterization was common equiatomic NiTi (cold rolled to 30% reduction in thickness, heat treated for 1 hour at 400 °C, quenched). Nominally isothermal mechanical loads were applied to tensile specimens at various temperatures. Lower temperature loading below A_s ($T < 100$ °C) led to the initiation and completion of stress-induced phase transformation followed by yielding of the material. Higher temperatures (100 °C $< T < 170$ °C) increased the stability of austenite such that mechanical loading led to plastic slip prior to the initiation of stress-induced transformation. Loading continued such that most or all of transformation was completed. Upon unloading, little or no reversed transformation was observed, and the total non-recovered strain consisted of both plastic and transformation components (cf. (2.2)).

The unloading step was followed by a slow heating to assess the possible effects that plastic strain generation might have on the thermal recovery behavior of the material. The reduction in recoverable strain and the shift in temperature required to initiated and complete transformation were noted. The entire series of loading/unloading/thermal recovery results is summarized in Figure 2.

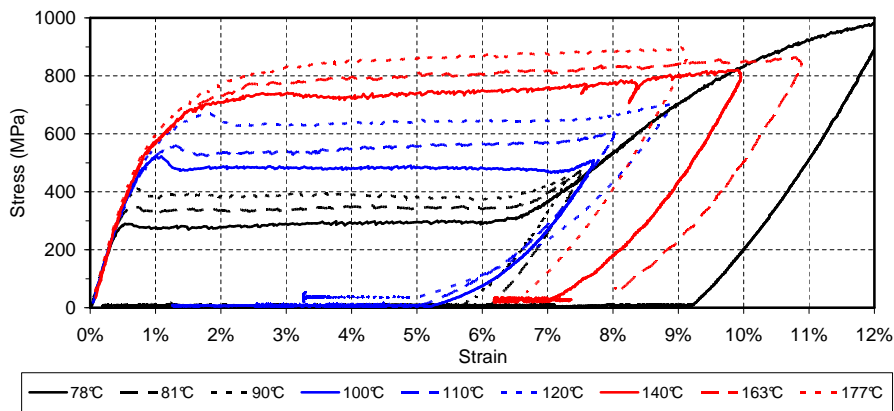


Figure 2. Series of uniaxial tensile results at various nominally constant test temperatures, including subsequent thermal strain recovery.

3.2. Calibration of the Model and Simulation of Experiments

The uniaxial tensile experimental results were then used to calibrated the 3-D constitutive model as implemented in the FEA framework.

- The *elastic properties* were determined by assessing the austenite elastic modulus during loading and the martensitic modulus during unloading. A standard Poisson’s ratio was assumed.
- The *transformation properties* of interest were the amount of transformation strain generated and fully recovered during non-yielding experiments at lower temperatures and the critical stress for transformation at various temperatures (i.e., the phase diagram).
- The *pure phase plastic properties* consisted of the initial yield stresses and plastic hardening behavior of austenitic yielding (at highest temperatures) and martensitic yielding (after completion of forward transformation).
- The *transformation/yielding coupling properties* were limited to the kinematic hardening parameters for each phase. These were most easily calibrated by assessed the effects of plastic strain on subsequent transformation temperatures (by way of the internal or “back stresses” induced).

By considering the averaged results of 10 total experiments ($78^\circ\text{C} < T < 177^\circ\text{C}$), appropriate material parameters were found and the model was fully calibrated. It is important to note that these calibrated material properties were not changed at any time during subsequent analysis. To validate the ability of the model to capture trends in material behavior, four of the calibration experiments (four different testing temperatures) were chosen for simulation. The numerically implemented constitutive model in the 3-D FEA framework was used to model the uniaxial tension boundary value problem. The applied thermomechanical loading paths (temperatures and applied strains) were intended to match the experimental conditions as closely as possible. The simulation results are compared to the experimental results for $T = 80^\circ\text{C}$, 110°C , 145°C , and 163°C in Figure 3. Note the very close agreement overall, including the increase in hardening during simultaneous transformation/yielding and accurate prediction of irrecoverable transformation strain as a consequence of plastic yielding.

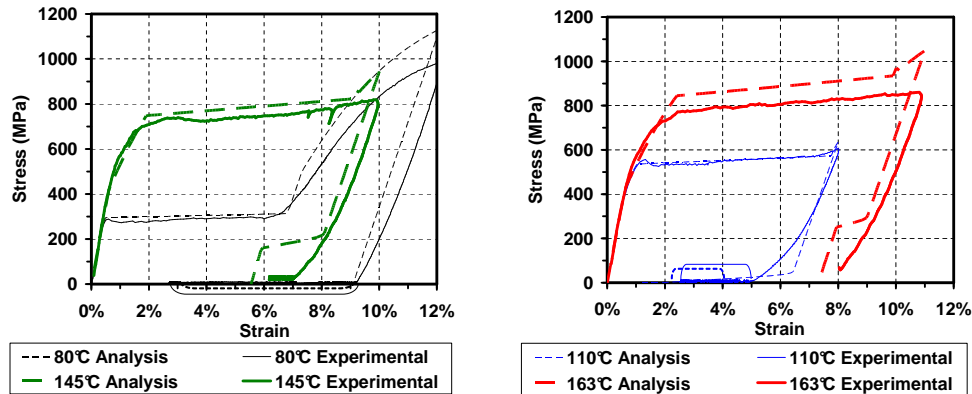


Figure 3. Selection of uniaxial tensile results at four nominally constant test temperatures and comparison with model simulation.

3.3. Numerical Analysis

To conclude this work, the 3-D analysis of an SMA body undergoing thermomechanical loading sufficient to induce simultaneous transformation and yielding is briefly reviewed. Specifically the loading consisted of subjecting a tensile “dogbone” specimen to three-point bending loads at high temperature. The specimen configuration and

material was the same as that used to produce the results shown in Figure 2 and thus the model calibration remained unchanged from simulation shown in Figure 3. The temperature during the application of bending loads was $T = 133\text{ }^{\circ}\text{C}$, which represents a temperature for which tensile experimental data was *not* generated.

The results for the distributed effective plastic strain and martensitic volume fraction at the end of loading as well as a comparison in predicted center force/deflection response with experimental results is shown in Figure 4. In comparing the predictions of the analysis to the experiment, it should be noted that the complicated experimental boundary conditions pertaining to the three-point loading fixture were not exactly replicated in the analysis. Considering this, the qualitative response prediction, especially with regards to irrecoverable deformation, is clearly of sufficient accuracy to be beneficial in engineering application design and analysis.

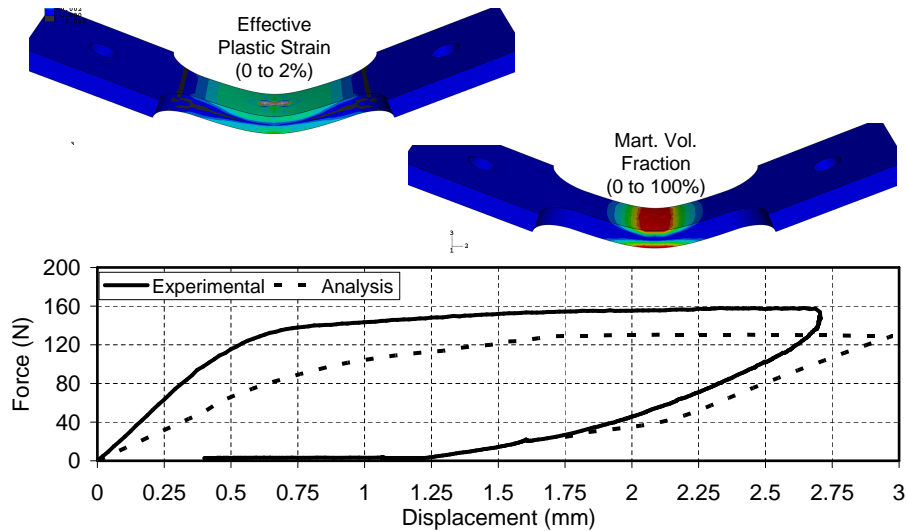


Figure 4. 3-D numerical analysis of simultaneous transformation/yielding in an SMA tensile specimen under bending loads.

ACKNOWLEDGMENTS

The authors would foremost like to acknowledge NASA-Glenn for their financial and technical support of this research (NASA Cooperative Agreement NNX07AB56A). Further funding for the work of D. Hartl is provided by the Integrative Graduate Education and Research Traineeship (IGERT) program administered by the National Science Foundation. Numerical analysis was performed through the use of an academic research license granted by ABAQUS, Inc.

REFERENCES

1. K. Otsuka and C. M. Wayman, eds., *Shape Memory Materials*, Cambridge University Press, Cambridge, 1999.
2. D. Lagoudas, ed., *Shape Memory Alloys: Modeling and Engineering Applications*, Springer-Verlag, 2008.
3. R. Noebe, T. R. Quackenbush, and I. Padula, S.A., “Benchtop demonstration of an adaptive chevron completed using a new high-temperature shape-memory alloy,” Tech. Rep. 20060054078, NASA, Glenn Research Center, May 2006.
4. Z. Bo and D. C. Lagoudas, “Thermomechanical modeling of polycrystalline SMAs under cyclic loading, Part III: Evolution of plastic strains and two-way shape memory effect,” *International Journal of Engineering Science* **37**, pp. 1175–1203, 1999.
5. D. C. Lagoudas and P. B. Entchev, “Modeling of transformation-induced plasticity and its effect on the behavior of porous shape memory alloys. Part I: Constitutive model for fully dense SMAs,” *Mechanics of Materials* **36**(9), pp. 865–892, 2004.
6. A. Paiva, M. A. Savi, A. M. B. Braga, and P. M. C. L. Pacheco, “A constitutive model for shape memory alloys considering tensile-compressive asymmetry and plasticity,” *International Journal of Solids and Structures* **42**(11–12), pp. 3439–3457, 2005.
7. X. Feng and Q. Sun, “Shakedown analysis of shape memory alloy structures,” *International Journal of Plasticity* **23**, pp. 183–206, 2007.
8. W. Yan, C. Wang, X. Zhang, and Y. Mai, “Theoretical modeling of the effect of plasticity on reverse transformation in superelastic shape memory alloys,” *Material Science & Engineering A* **A354**, pp. 146–157, 2003.
9. X. Wang, B. X. Xu, and Z. Yue, “Micromechanical modelling of the effect of plastic deformation on the mechanical behavior in pseudoelastic shape memory alloys,” *International Journal of Plasticity*, 2007. In press.
10. D. C. Lagoudas, Z. Bo, and M. A. Qidwai, “A unified thermodynamic constitutive model for SMA and finite element analysis of active metal matrix composites,” *Mechanics of Composite Materials and Structures* **3**, pp. 153–179, 1996.
11. Dassault Systmes of America Corp., Woodlands Hills, CA, *ABAQUS/Standard User’s Manual*, 2006.
12. M. A. Qidwai and D. C. Lagoudas, “Numerical implementation of a shape memory alloy thermomechanical constitutive model using return mapping algorithms,” *International Journal for Numerical Methods in Engineering* **47**, pp. 1123–1168, 2000.
13. B. D. Coleman and M. E. Gurtin, “Thermodynamics with internal state variables,” *The Journal of Chemical Physics* **47**, pp. 597–613, July 1967.
14. J. C. Simo and T. J. R. Hughes, *Computational Inelasticity*, vol. 7 of *Interdisciplinary Applied Mathematics*, Springer-Verlag, New York, 1998.
15. M. A. Qidwai and D. C. Lagoudas, “On the thermodynamics and transformation surfaces of polycrystalline NiTi shape memory alloy material,” *International Journal of Plasticity* **16**, pp. 1309–1343, 2000.
16. G. Houslsby and A. Puzrin, *Principles of Hyperplasticity*, Springer-Verlag, 2006.
17. A. McKelvey and R. Ritchie, “Fatigue-crack growth behavior in the superelastic and shape-memory alloy nitinol,” *Metallurgical and Material Transactions A* **32**(13), pp. 731–743, 2001.
18. V. Brailovski, S. Prokoshkin, P. Terriault, and F. Trochu, eds., *Shape Memory Alloys: Fundamentals, Modeling, and Applications*, University of Quebec, 2003.